Chapter 5
Building Porosity for Better Urban Ventilation in High-Density Cities

5.1 Introduction

5.1.1 Background

Nowadays, cities are homes to over half of the world's population, and the city population is expected to reach 4.96 billion by 2030 (United Nations Population Division 2006). Urbanization improves living quality but also spontaneously increases the demand on natural resources (World Wildlife Fund (WWF) 2010). To address such urbanization issue, high-density living that enables cities to utilize resources more efficiently by decreasing traffic cost and other energy usage is a viable alternative (Betanzo 2007). However, high-density living may lead to congested urban conditions, which in term are associated with serious environmental issues, such as poor outdoor natural ventilation (Ng 2009a). Taking Hong Kong as an example, the extremely rapid and successful growth of Hong Kong in the last century had led to the increase of high-rise compact buildings and deep street canyons (Fig. 5.1), which significantly block airflow in the urban canopy layer (Fig. 5.2).

Stagnant air at urban areas is associated with both outdoor urban thermal discomfort and increased air pollution. Outdoor thermal comfort under typical summer conditions requires 1.6 m/s wind speed; however, a decrease in wind speed from 1.0 to 0.3 m/s during the summer could result in 1.9 °C increase in temperature (Cheng et al. 2011). Wind data from urban observatory station of Hong Kong Observatory (HKO) indicates that the mean wind speed at 20 m above the ground level in a urban area (i.e., Tseung Kwan O) has decreased by about 40%, from 2.5 to 1.5 m/s over the past

Originally published in Chao Yuan and Edward Ng, 2012. Building porosity for better urban ventilation in high-density cities–A computational parametric study. Building and Environment, 50, pp.176–189, © Elsevier, https://doi.org/10.1016/j.buildenv.2011.10.023.

C. Yuan, *Urban Wind Environment*, SpringerBriefs in Architectural Design and Technology, https://doi.org/10.1007/978-981-10-5451-8_5

decade (Hong Kong Planning Department (HKPD) 2005). Due to poor dispersion, frequent occurrences of high concentrations of pollutants, such as NO_2 and respirable particles (RSP), in urban areas like Mong Kok and Causeway Bay have been reported by the Hong Kong Environmental Protection Department (Yim et al. 2009b).

The 2003 outbreak of the Severe Acute Respiratory Syndrome (SARS) epidemic in Hong Kong had brought attention to how environmental factors (i.e., air ventilation and dispersion in buildings) played an important role in the transmission of SARS and other viruses. Since the outbreak, the Hong Kong Special Administrative Region (HKSAR) Government strived to improve the local wind environment for better urban living quality. Relevant studies, policies, and technical guidelines, such as Air Ventilation Assessment (AVA) and Sustainable Building Design (SBD) Guidelines, have been conducted and applied on the urban planning and design process (Ng 2009b). The Hong Kong Planning Department (HKPD) initiated the "Feasibility study for establishment of Air Ventilation Assessment system" in 2003 to answer the fundamental question of "*how to design and plan our city fabric for better natural air ventilation?*" (HKPD 2005). In that study, the current air ventilation issues in Hong Kong were provided, and the corresponding qualitative urban design methodologies and guidelines were given in order to create an acceptable urban wind environment. Unlike AVA, the SBD Guidelines (under APP-152 of Buildings Department HKSAR) are intended for building scale, providing the quantitative requirements for three building design elements, namely, building separation, building set back, and site coverage of greenery. The SBD Guidelines (1) aim to mitigate the negative effects of new building development on the existing surrounding wind environment, (2) enhance the environmental quality of living spaces in Hong Kong, and (3) enable architects to mitigate the undesirable effect of new buildings without needing CFD simulation and wind tunnel experiments by modifying simple design indexes (e.g., building length, distance to the adjunct streets or site boundary, width of the building gap, and size of wind permeability) from the Guidelines.

The computational parametric study described in this chapter aims to quantify the SBD Guidelines by evaluating the effect of mitigation strategies on improving urban wind environment. Scientific evidence-based understandings are provided in order to choose appropriate design strategies that can efficiently improve the pedestrian-level natural ventilation while preserving land use efficacy. As shown in Fig. 5.3, Mong

Fig. 5.1 View of the Kowloon Peninsula and Hong Kong Island in the 1900s and today (Waller 2008; Moss 2008)

Fig. 5.2 High-rise compact building blocks and deep street canyons in Hong Kong (Wolf 2009)

Fig. 5.3 Urban fabric of Mong Kok: the grid plan

Kok, one of metropolitan areas in Hong Kong, is chosen as the case study to represent regular street grid planning, which is widely applied in mega cities planning, such as Manhattan, and Philadelphia in the U.S.

5.2 Literature Review

5.2.1 *Outline of CFD Numerical Methods for Neutral Turbulence Flows*

The rapid development of CFD application in environmental design in the past three decades is remarkable. Not only is CFD a well-established environmental research tool to enhance our predictive power, it is also a recognized design tool for urban planners and designers (Murakami 2006). With CFD, highly unsteady and three-dimensional turbulent flows in the atmospheric boundary can be simulated. In the following sections, three main CFD methods, which are Direct Numerical Simulation (DNS), Large Eddy Simulation (LES), and Reynolds-averaged Navier–Stokes (RANS) are discussed.

Compared with laminar flows, the fluctuation of turbulent flows is on a broad range of spatial and temporal scales (Ferziger and Peric 2002; Murakami 2006). In DNS, all spatial and temporal scales of the turbulence motions are directly computed by Navier–Stokes equations without any approximations by turbulence models (Ferziger and Peric 2002). Because of this, DNS is the most accurate among all of the simulation methods. However, using the DNS model to totally reproduce turbulence is extremely expensive. On the other hand, the LES method separates the turbulence flow into large and small scales, and only focuses on the "large eddy" that is larger than grid size. Small eddies, such as eddies in Kolmogorov scales, are eliminated from the solution to reduce computational cost. The unresolved scales of turbulence flows are approximated by the sub-filter-scale turbulence models (Meneveau and Katz 2000; Kleissl and Parlange 2004). As a result, LES is computationally cheaper than DNS, and has been used as a research tool in a wide range of engineering applications to simulate high Reynolds flows, such as simulations of the neutral atmospheric boundary layer (Letzel et al. 2008).

Unlike the DNS and LES methods, which are time-dependent approaches, the RANS method does not directly compute any turbulence by Navier–Stokes equations, but rather approximates the turbulence flows by decomposing solution variables in DNS and LES into the time-averaged and fluctuating components:

$$f = <f> + f' \tag{5.1}$$

where f is the instantaneous value of variables, such as velocity, in the Navier–Stokes equations, $<f>$ is the mean value, and f' is the fluctuating value. The turbulence models are to approximate the effects of f'. Therefore, compared with DNS and LES, RANS is a simplified engineering approximation that has been broadly applied as a design tool.

The computational parametric study described in this chapter applies the RANS method to simulate the wind velocity in the neutral condition. Reynolds-averaged equations are yielded by substituting Eq. (5.1) to the Navier–Stokes equations. The

incompressible flow equations with constant density (ρ), i.e., airflow in this study, can be written as follows:

$$\text{Continuity equation}: \quad \frac{\partial < u_i >}{\partial x_i} = 0 \tag{5.2}$$

$$\text{Momentum equation}: \quad \frac{D < u_i >}{Dt} = -\frac{1}{\rho} \cdot \frac{\partial < P >}{\partial x_i} + \frac{\partial}{\partial x_j} \left(v \frac{\partial < u_i >}{\partial x_j} - < u_i' u_j' > \right), \tag{5.3}$$

where x_i ($i = x, y, z$) are the coordinates, u_i are velocity vectors, t is time, v is dynamic viscosity, and p is pressure. Equations (5.2) and (5.3) are similar with the Navier–Stokes equations, except that all variables are time averaged, and the Reynolds stresses, $-<u_i' u_j'>$, must be approximated by turbulence models to close Equations.

According to the various approaches of dealing with Reynolds stresses, $-<u_i' u_j'>$, the RANS model can be classified into two types: (a) Boussinesq Approach–turbulence viscosity ($\kappa - \varepsilon$ and $\kappa - \omega$ turbulence models) and (b) Reynolds Stress Models (RSM). The RSM turbulence model, as an anisotropic model, considers the effects of Reynolds stress by using six equations to compute $-<u_i' u_j'>$ directly. Compared to the $\kappa - \varepsilon$ and $\kappa - \omega$ turbulence models, where ε (turbulence dissipation rate) or ω (the specific dissipate rate) is assumed isotropic, RSM is more computationally costly. However, RSM is more accurate than the $\kappa - \omega$ realized model in flows with strong anisotropic effects (i.e., swirling flows) (Kuznik et al. 2007). On the other hand, the accuracy of RSM is similar to the models by Boussinesq Approach in normal flows (Wong 2004).

Current commercial CFD codes provide both turbulence viscosity model and RSM models. In our computational parametric study, the $\kappa - \omega$ SST (Shear Stress Transport) models were applied. The $\kappa - \omega$ SST model is a combination of the standard $\kappa - \omega$ model and $\kappa - \varepsilon$ model. Walls are the main source of turbulence; therefore, an accurate near-wall treatment is critical for turbulence models to be useful (Fluent 2006). While the standard $\kappa - \omega$ model, as a near-wall model, is more accurate than the $\kappa - \varepsilon$ models in the near-wall layers (Menter et al. 2003), it cannot replace the $\kappa - \varepsilon$ models in the simulation of the outer part of the near-wall region (Menter et al. 2003). The $\kappa - \omega$ SST model uses the standard $\kappa - \omega$ model for the inner part and gradually changes to the $\kappa - \varepsilon$ model for the outer part (Menter et al. 2003; Fluent 2006).

5.3 Validation

Cross-comparisons of wind data from RANS ($\kappa - \varepsilon$ models), DES, LES, and the wind tunnel experiments were conducted by a working group from the Architectural Institute of Japan (AIJ) to calibrate the CFD simulation results (Tominaga et al.

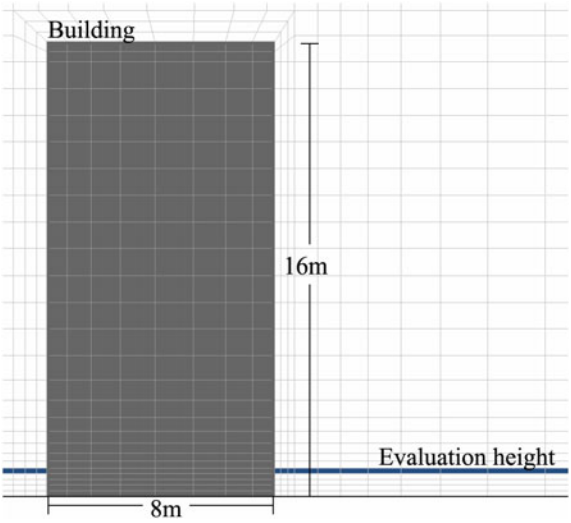

Fig. 5.4 Grid structure and resolution. The maximum grid size ratio is 1.2 and four mesh layers are arranged below the evaluation height

2008; Mochida et al. 2002). In this chapter, the SST $\kappa - \omega$ model was validated by comparing the simulation results with the wind tunnel data from AIJ. Menter et al. (2003) compared the simulation results obtained from the $\kappa - \omega$ SST and DES SST models. The data for comparison was a set of vertical mean wind velocity profiles across a single cubic block. The result suggests that while the $\kappa - \omega$ SST model can predict airflow near the building, it fails to reproduce the recovery downstream in the separation zone that is far from the building (Menter et al. 2003). Since our study mainly focuses on the pedestrian-level wind environment, both the pedestrian-level wind speed distribution and vertical wind velocity profiles are compared with the data derived from the wind tunnel experiment.

CFD simulation settings for the validation and parametric study follow AIJ guidelines for urban pedestrian wind environment modeling. The size of computational domain and building block in the validation study are 500 × 500 × 60 m and 8 × 8 × 16 m ($W \times L \times H$), respectively. As shown in Fig. 5.4, adaptive meshing method is applied to reduce computational cost, and accurately predicted wind speed at the areas of interest. The finer scale grids are arranged at the areas around the building and close to the ground (Fig. 5.4). To comply with the AIJ guidelines, four layers (layer height: 0.5 m) are arranged below the evaluation height (2.25 m above the ground). The maximum grid size ratio is set to 1.2, as shown in Fig. 5.4.

In terms of input boundary condition, the vertical wind speed profile is set to

$$U_{(h)} = U_{\text{met}} \cdot \left(\frac{h}{d_{\text{met}}} \right)^{\alpha}, \tag{5.4}$$

where α is the surface roughness factor $\alpha = 0.2$ U_{met} is the wind speed at the top of the domain ($U_{\text{met}} = 6.751$ m/s), d_{met} is the domain thickness ($d_{\text{met}} = 60$ m), and h

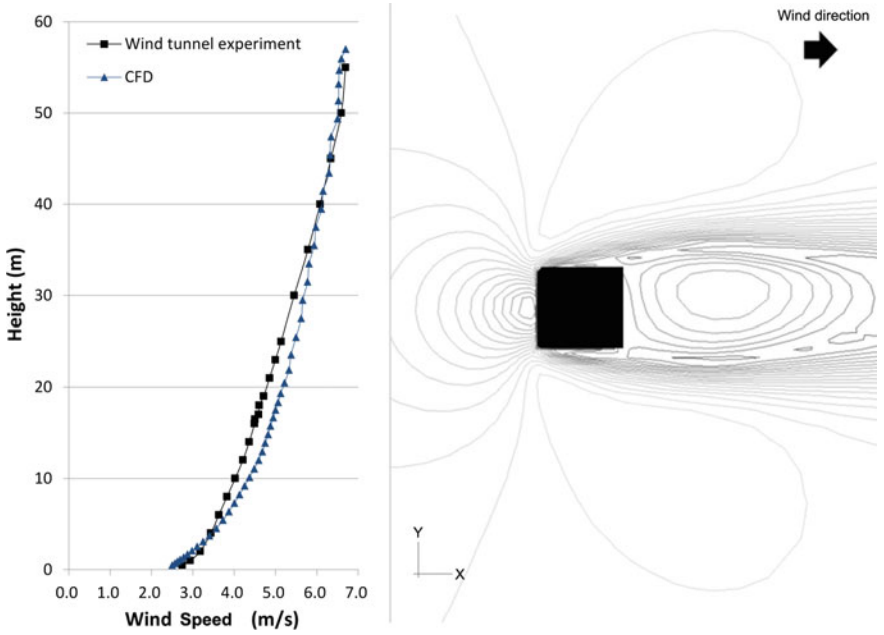

Fig. 5.5 Inlet mean wind speed profiles in the CFD simulation and wind tunnel experiment, and the simulation result (the contour of wind speed at 2.25 m above the ground)

is the height. To compare with data from the wind tunnel experiment, the inlet wind profile in CFD simulation is set similarly as possible to the one from the wind tunnel experiment, as shown in Fig. 5.5.

The contour of wind speed at 2.25 m above the ground is presented in Fig. 5.5. Figure 5.6 shows the position of the test points and cross-comparing result (R^2 = 0.853), which indicates that the $\kappa - \omega$ SST model can accurately predict the pedestrian-level airflow within urban context. To further validate the simulation results, the vertical profiles of the mean wind velocities from CFD simulation and wind tunnel experiment at position 1 and position 2 (depicted in Fig. 5.6) are also presented in Fig. 5.7. The results are consistent with the experiment results produced by Menter et al. (2003).

5.4 Computational Parametric Study

In this section, a parametric approach is applied to obtain more general understandings on wind performance with particular building typologies, and to identify the effects of individual design parameters on natural ventilation performance more easily than do conventional studies (Mochida et al. 1997; Kondo et al. 2006; Ashie et al. 2009). Specifically, three groups with 27 testing scenarios are set up in three

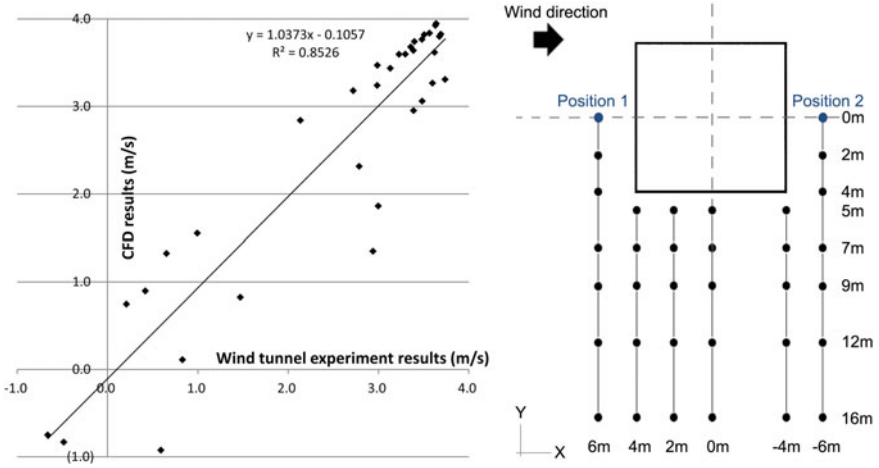

Fig. 5.6 Test points and the linear correlation of wind speeds from the CFD simulation and wind tunnel experiment (significant level: 0.95)

input wind directions, and are simulated by the $\kappa - \omega$ SST model. The following section will introduce the building model design, computational modeling of the testing scenario, and boundary conditions in this computational parametric study.

5.4.1 Parametric Models

To evaluate the effect of urbanization on urban natural ventilation and to predict future conditions, three design scenarios (i.e., Cases 1903, 1, and 2) are designed based on the urban morphologies of the past, present, and future Mong Kok, a metropolitan area that has significantly changed overtime. Compared with Mong Kok in 1903, the population density in present day Mong Kok is extremely high, reaching 130,000/km^{-2} (Wikipedia 2011). Given the current planning trend, the population density of this downtown area in the future will be much higher. Case 1903 refers to the past Mong Kok characterized by three or four-floor buildings with a sloping roof. In a simplified parametric model, the sloping roof is replaced by a flat floor and 20 m building height. Case 1 refers to the present day Mong Kok in which the height of buildings and podiums is on average 45 and 15 m, respectively (Ng et al. 2011). The site area is not fully occupied, with narrow gap in between. Case 2 refers to future Mong Kok in which the height of buildings on average is estimated to increase to 90 m. The site area will be fully occupied in response to the increasing urban land use.

Six design options with various building typologies are tested to see the effects of different building typologies on pedestrian-level natural ventilation performance in order to identify efficient mitigation strategies. As shown and summarized in Fig. 5.8, mitigation strategies include: (a) setting back buildings, (b) separating the

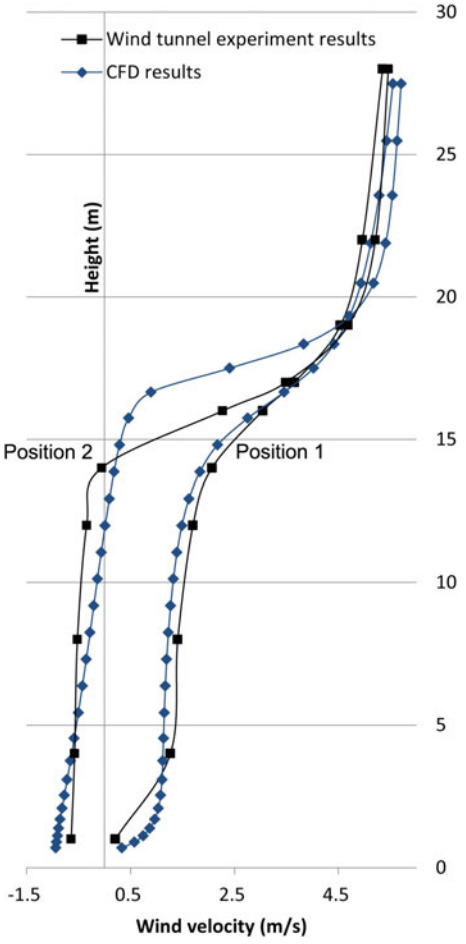

Fig. 5.7 Vertical profiles of the mean wind velocities from the CFD simulation and wind tunnel experiment. Locations of the vertical lines: Position 1 (windward) and 2 (leeward)

long buildings, (c) stepping the podium, (d) opening the permeability of towers and podiums, and (e) creating a building void between towers and podiums. In Cases 3–7, the building volumes are similar to the one in Case 2 to keep the land use density constant.

Case 3 is similar to Case 2, except that the building set back is 15 m along the street in Case 3. Case 3 shows that setting back buildings is relatively easy to be applied in urban planning. Building separations along the prevailing wind direction are applied in Case 4. The decreased land use efficiency resulting from the building separations is compensated by higher towers (123 m). Case 5 is the combination of Cases 3 and 4. The stepped podium and building void in Case 6 are popular design strategies in Hong Kong, which are favorable for natural outdoor ventilation and greening. Air passages in high and wide buildings are applied in Case 7. This strategy is currently widely used in Hong Kong to mitigate the undesirable effects on the leeward wind environment.

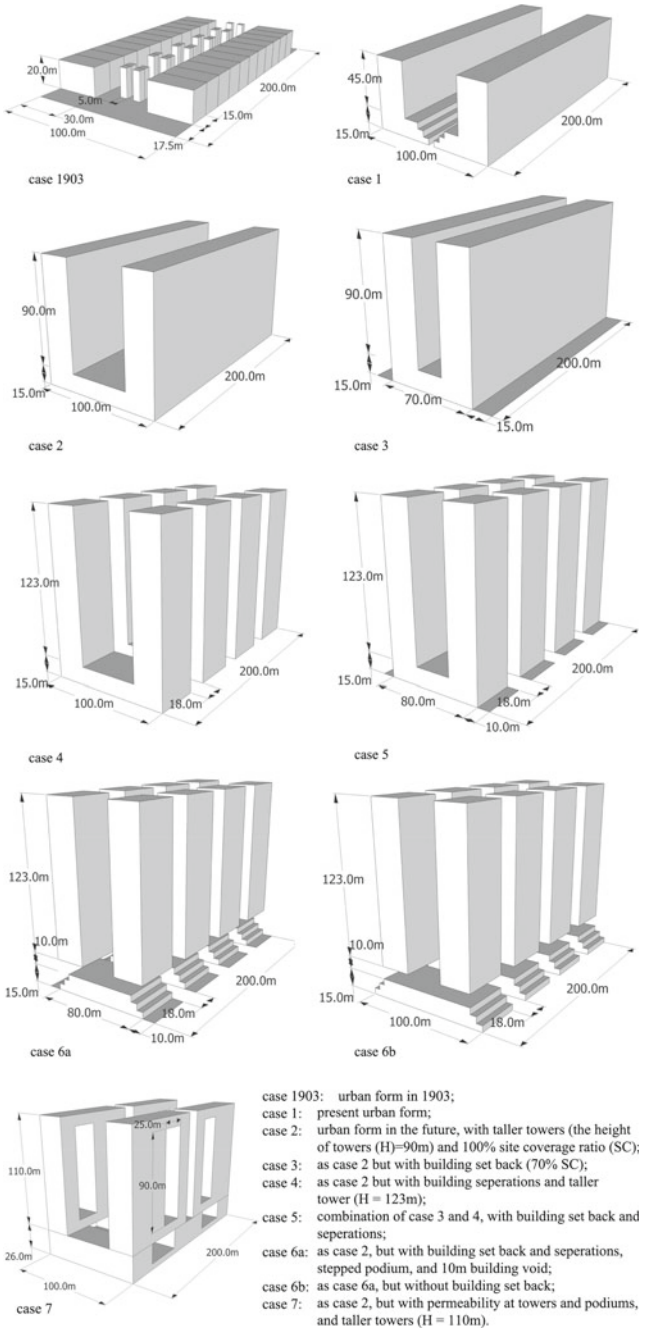

Fig. 5.8 Summary of nine testing models which are designed to test the effects of different building morphologies on natural ventilation performance

5.4.2 Computational Modeling

A computational modeling for neighborhood scale is used in the current parametric study. Several existing parametric studies for wind evaluation and prediction have focused on the airflow around only one or two simple and generic buildings (Stathopoulos and Storms 1986; To and Lam 1995; Blocken et al. 2007). However, the turbulence kinetic energy produced by the urban context is difficult to reproduce in the inlet boundary condition. The testing scenario modeled in the urban scale can approximately include the effect of urban context on airflow to evaluate and predict the natural ventilation performance in the area of interest more accurately.

In the current study, 27 testing scenarios are simulated in the neutral condition by the $\kappa - \omega$ SST model in three wind directions (0°, 45°, and 90°). As shown in Fig. 5.9, each testing scenario is made up of a corresponding model array (6×10) and two rows of surrounding randomized buildings. The same regular street grid is applied in all model arrays; the width of the street canyon is 20 m. To consider the effects of urban context, only the wind data measured at the target area (Fig. 5.9) are used in the numerical analysis.

The computational domain size is $3.2 \times 3 \times 0.45$ km ($W \times L \times H$), as shown in Fig. 5.9. The grid point numbers are 5.0–6.8 million on a case-by-case basis. Similar to the meshes in the validation study, the finer meshes are arranged at the areas around the buildings and close to the ground. To comply with the AIJ guideline, the maximum grid size ratio is set to 1.2, and the three grid layers (layer height: 1 m) are arranged below the evaluation level. This means that only the wind data at 3.5 m above the ground are collected and analyzed.

To set the inlet boundary condition for Mong Kok area by Eq. (5.4), the site-specific annual wind rose data measured at a 450 m height are obtained from the fifth-generation NCAR/PSU mesoscale model (MM5) (Yim et al. 2009a). As shown in Fig. 5.10, wind from east and northeast have higher and the highest probability of occurrence, respectively. Therefore, input prevailing wind direction in the simulation is set to 90°. Simulations in the input wind directions of 0° and 45° (Fig. 5.10) are also included to describe comprehensively the natural ventilation performance in different wind directions. Wind speed at the top of the domain is set to $U_{\text{met}} = 11$ m/s, which is the mean prevailing wind speed at a 450 m height in the summer. Owing to the high urban surface roughness, surface roughness factor (α) is set to 0.35 in this computational parametric study. The outlet wind profile is set to be the same as the inlet wind profile.

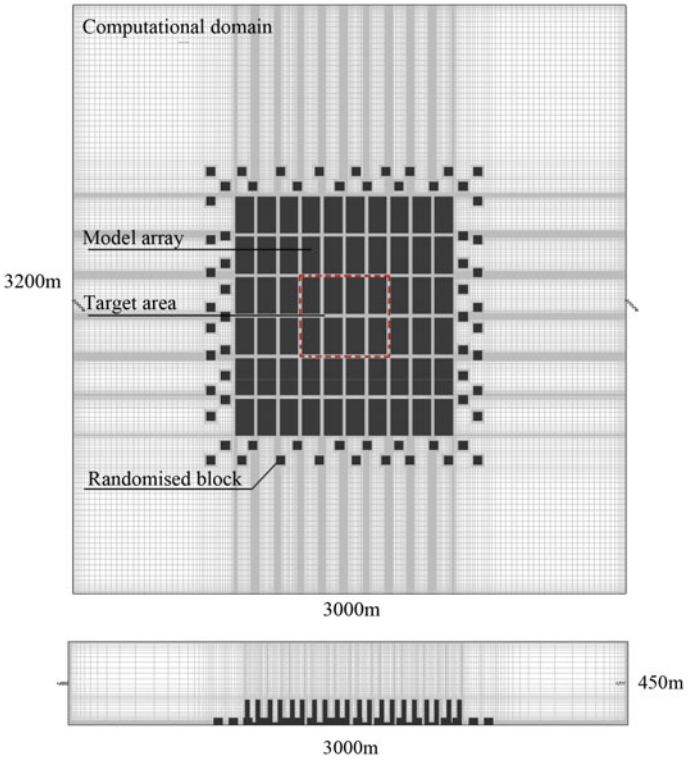

Fig. 5.9 Computational domain and grids for the parametric study. The model array, randomized block, and the target area are presented

5.5 Modeling Results and Analysis

5.5.1 Wind Speed Classification

A wind speed classification based on outdoor thermal comfort is derived to correlate the building design options with outdoor thermal comfort. Different from the classification by Beaufort (cited in Cheng and Ng 2006) and Murakami and Deguchi (1981), in which wind is a kind of "nuisance", the current parametric study considers wind as a benefit. Therefore, this classification is based on the outdoor thermal comfort and not on the wind force on pedestrians or buildings. Ng et al. (2008) conducted a survey to use physiological equivalent temperature (PET) to obtain the pedestrian-level wind speed threshold values, especially for outdoor thermal comfort in Hong Kong (Hoppe 1999). This survey showed that a wind speed of 0.6–1.3 m/s was required to achieve neutral thermal sensation (neutral PET: 28.1 °C) in a typical summer day with ambient temperature of 27.9 °C and relative humidity of 80%. In another survey on thermal comfort in Hong Kong (Cheng et al. 2011), the wind speed settings

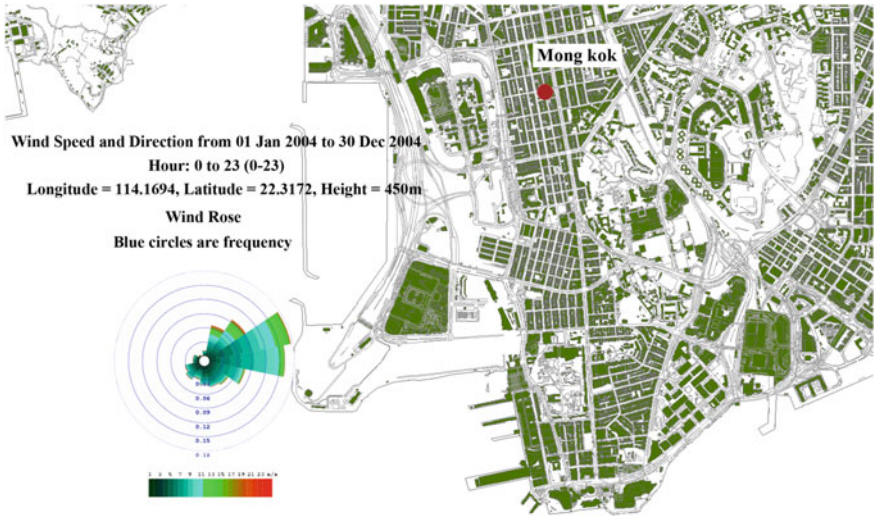

Fig. 5.10 Site-specific annual wind rose of Mong Kok

with and without wind break were 0.3 m and 1.0 m, respectively, which equaled to a 1.9 °C difference in ambient temperature. Based on this literature review, the classification of pedestrian-level wind speed (u) is assigned as the following: Class 1: $u < 0.3$ m/s for "stagnant," Class 2: 0.6 m/s $> u \geq 0.3$ m/s for "poor," Class 3: 1.0 m/s $> u \geq 0.6$ m/s for "low," Class 4: 1.3 m/s $> u \geq 1.0$ m/s for "satisfactory," and Class 5: $u \geq 1.3$ m/s for "good" pedestrian-level natural ventilations in street canyons, respectively.

5.5.2 *Impact of Input Wind Directions*

The contour colored by mean wind speed in Case 1 is presented in Figs. 5.11 and 5.12. The accelerated wind speed is found at street canyons that are parallel with the input wind direction (wind direction 90°, Fig. 5.11). However, other than these areas, wind speed is significantly reduced in deep street canyons perpendicular to the wind direction. When the input wind direction is changed from 90° (Fig. 5.11) to 45° (Fig. 5.12, right), air can enter into the streets from both directions (Fig. 5.12), resulting in the decrease in areas with stagnant air. On the other hand, air can enter more deeply into the streets in the wind direction 0° (Fig. 5.12, left) than 90° (Fig. 5.11), due to the smaller frontal area (please refers to Chap. 2 for more details and definition of frontal area). The above discussion is consistent with the statement in the AVA study saying "*An array of main streets, wide main avenues and/or breezeways should be aligned in parallel, or up to 30 degrees to the prevailing wind direction, in order to maximize the penetration of prevailing wind through the district.*" (HKPD 2005).

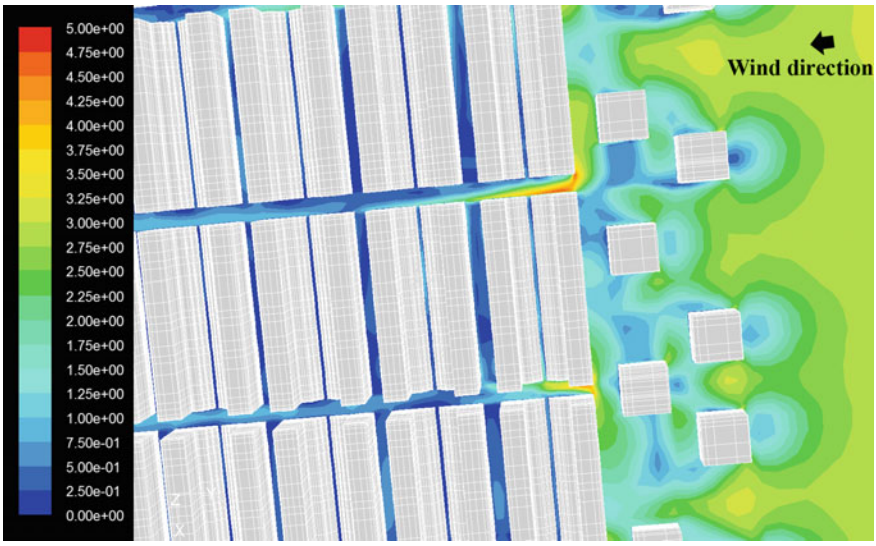

Fig. 5.11 Contour of wind speed in the wind direction of 90° (prevailing wind direction) at 3.5 m above the ground (Case 1). (For interpretation of the references to color in the text, the reader is referred to the electronic version of this book)

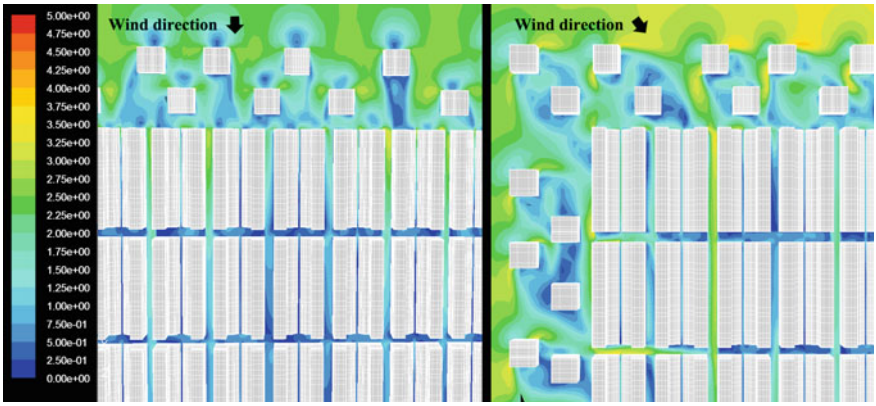

Fig. 5.12 Contours of wind speed in the wind direction of 0° (right) and 45° (left) at 3.5 m above the ground (Case 1). (For interpretation of the references to color in the text, the reader is referred to the electronic version of this book)

5.5.3 Impact of Building Typologies

A cross-comparison of natural ventilation performance in the prevailing wind direction of 90° is summarized in Figs. 5.13 and 5.14, and Table 5.1. Wind data are statistically analyzed based on the relative frequency of the wind speed classifica-

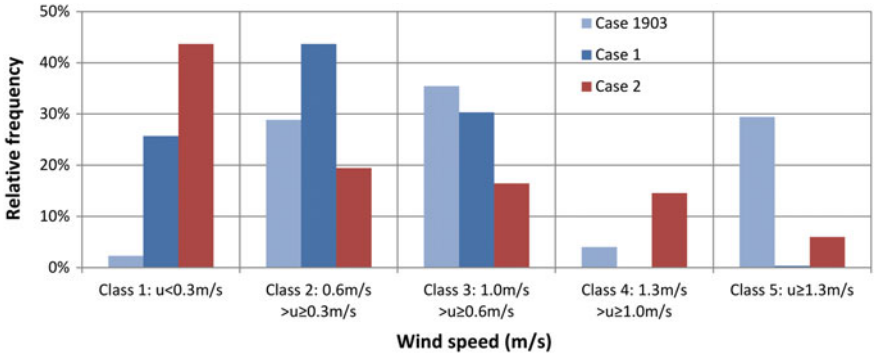

Fig. 5.13 Relative frequencies of pedestrian-level mean wind speed in Cases 1903, 1, and 2 (Input wind direction: 90°)

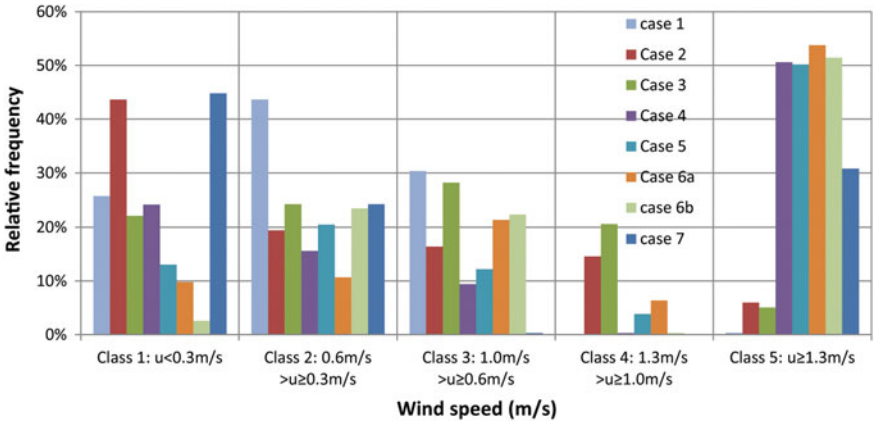

Fig. 5.14 Relative frequencies of the pedestrian-level wind speed in Cases 1, 2, 3, 4, 5, 6a, 6b, and 7 (Input wind direction: 90°)

tion. About 300 wind speed data in every test scenario are collected at the centerlines of four streets in the target area (Fig. 5.9). Figure 5.13 shows the evaluation of natural ventilation performance of the past (Case 1903), present (Case 1), and future (Case 2) Mong Kok. For area with very poor natural ventilation (Class 1: $u < 0.3$ m/s), Case 1903 accounts for the lowest frequency (2.29%), whereas Cases 1 and 2 account for 25.67 and 43.67%, respectively. This is consistent with the rapid urbanization trend in the Mong Kok area in the last century.

The effects of design options with various mitigation strategies (Cases 3–7) on the urban natural ventilation performance are presented in Fig. 5.14. First, building setbacks (Case 3) and building separations (Case 4) are helpful in improving pedestrian-level natural ventilation. Compared with Case 2, the relative frequencies of very poor ventilation (Class 1) in Cases 3 and 4 reduce to 22.02 and 24.12%, respectively. However, the wind performances in Cases 3 and 4 still resemble that in

Table 5.1 Summary of the relative frequencies of pedestrian-level wind speed in nine testing models (input wind direction: 90°)

	$u < 0.3$ m/s	0.6 m/s $> u \geq 0.3$ m/s	1.0 m/s $> u \geq 0.6$ m/s	1.3 m/s $> u \geq 1.0$ m/s	$u \geq 1.3$ m/s
	Stagnant (%)	Poor (%)	Low (%)	Satisfactory (%)	Good (%)
Case 1903	2.29	28.86	35.43	4.00	29.43
Case 1	25.67	43.67	30.33	0.00	0.33
Case 2	43.66	19.40	16.42	14.55	5.97
Case 3	22.02	24.19	28.16	20.58	5.05
Case 4	24.12	15.59	9.41	0.29	50.59
Case 5	13.06	20.47	12.17	3.86	50.45
Case 6a	9.83	10.69	21.39	4.34	53.76
Case 6b	2.60	23.41	22.25	0.29	51.45
Case 7	44.78	24.18	0.27	0.00	30.77

Case 1 (the current urban wind environment), and thus are deemed to be suboptimal. Second, the relative frequency of Class 1 is decreased further to 13.06% in Case 5, in which both building setbacks and separations are adapted. Third, stepped podiums and 10 m building voids are applied in Cases 6a and 6b. The relative frequency of Class 1 in Case 6a and Case 6b is 9.83 and 2.60%, respectively, which indicate good natural ventilation performance similar to Case 1903, even though the land use density in Case 6 is higher than that in Case 1903. Last but not least, air passages in the tower and podium are applied in Case 7, with very high relative frequency (44.78%) in Class 1 remaining.

Furthermore, two similar analyses are conducted for the cases in the input wind directions of 0° and 45°. First, as shown in Figs. 5.15 and 5.16, the relative frequencies of good natural ventilation performance reach to 80%, which indicates that the modification of street grid direction is helpful in improving natural ventilation performance. Second, the natural ventilation performance becomes less sensitivity to the changes in building morphologies in these two input wind directions, especially in the 45° input wind direction.

5.5.4 Comparison of the Vertical Wind Profiles

The vertical profiles of the mean wind velocity are collected at a point on the centerline of the street across the prevailing wind direction, and they are plotted in Fig. 5.17 to help better understand the above analysis results. Figure 5.17a shows the profiles from 0 to 400 m, indicating that building height significantly affects wind profiles, especially at $z_d + z_0$ values. The height of zero velocity in the wind profiles is close to but slightly lower than the mean height of buildings. This result is consistent with

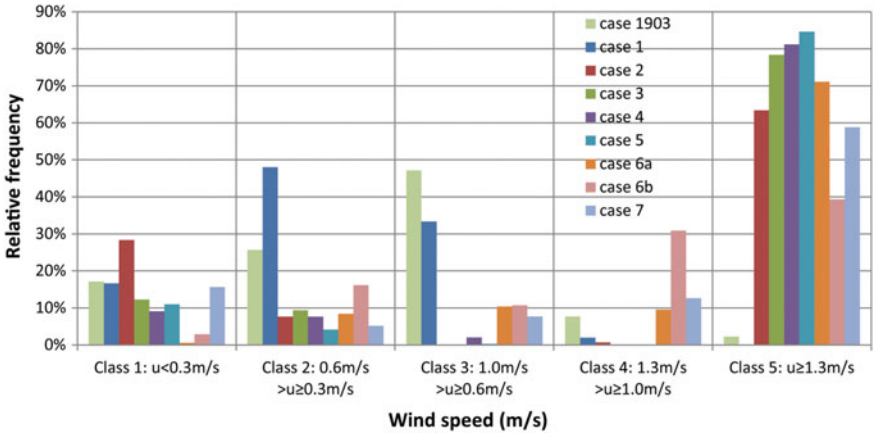

Fig. 5.15 Relative frequencies of the pedestrian-level wind speed in Cases 1903, 1, 2, 3, 4, 5, 6a, 6b, and 7 (Input wind direction: 0°)

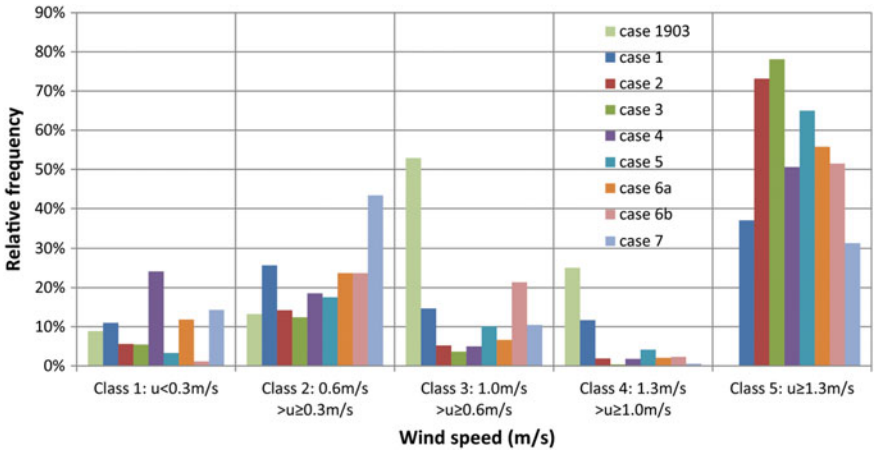

Fig. 5.16 Relative frequencies of the pedestrian-level wind speed in Case 1903, 1, 2, 3, 4, 5, 6a, 6b, and 7 (Input wind direction: 45°)

that of Oke (2006) and Lawson (2001). The profiles from 0 to 50 m are enlarged in Fig. 5.17b to show airflow that is closer to the ground. Our results indicate that the wind environment at the pedestrian level is not affected by building height, but rather is significantly influenced by building morphology in the podium layer. The results agree with the frontal area density study in the urban scale by Ng et al. (2011).

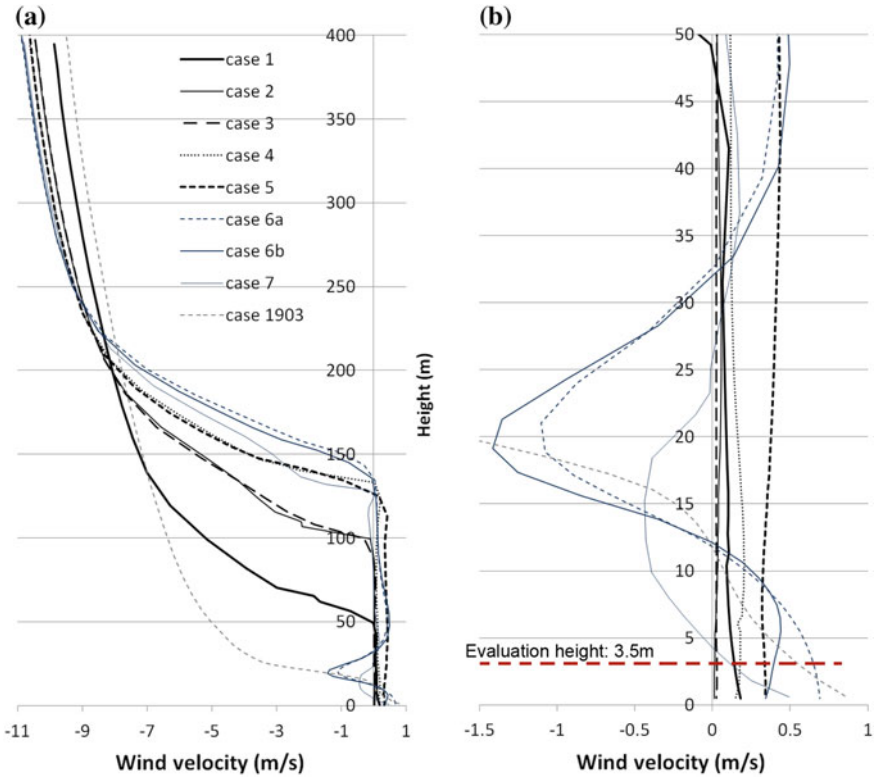

Fig. 5.17 Mean wind velocity profiles measured at the centerline of the street canyon across the wind direction

5.6 Conclusion

This chapter presents a computational parametric approach for evaluating the effects of different urban morphologies on the pedestrian-level natural ventilation environment through CFD simulation. Different simulation methods and turbulence models are compared based on the literature review. The $\kappa - \omega$ SST turbulence model is applied in this study. Results of the comparison between CFD simulation results and wind tunnel data suggest that the $\kappa - \omega$ SST turbulence model is accurate enough to simulate the turbulent flows caused by shape-edged buildings. Unlike the wind field studies in real urban areas, our study designs a number of parametric models to test the different modification effects on pedestrian-level air flow in street canyons. Compared with other parametric studies in which only one or two buildings are included, this study employs computational modeling in the urban scale to include the effects of the urban context. This study derives a wind speed classification based on the outdoor thermal comfort, as well as uses the relative frequency of the pedestrian-level

wind speed and the vertical profiles of the mean wind velocity to evaluate the natural ventilation performance in street canyons. Cross-comparison results suggest that the sensitivity of the wind performance is not the same across different modifications of building morphology. Relevant planning and design strategies are provided based on the findings of this study as follows:

(1) Street grid orientation in grid planning is a significant parameter in urban natural ventilation performance. Main streets should be arranged along the prevailing wind direction. Efficiency of the design strategies also depends on the prevailing wind direction, as demonstrated in the results in Sect. 5.3.
(2) The mean building height determines the $z_0 + z_d$ value in high-density urban areas, while urban ventilation performance from the pedestrian perspective mostly depends on the pedestrian-level building porosity.
(3) Overall, decreasing the site coverage ratio increases the pedestrian-level natural ventilation performance. Comparison of Cases 3, 4, and 5 provides a more detailed understanding. The wind profiles in Cases 3 and 4 suggest that building setbacks along the street across the prevailing wind direction (Case 3) are less useful in high-density urban areas than building separations along the prevailing wind direction (Case 4). In contrast, the wind profiles in Case 5 (Fig. 5.8) suggest improvement of the pedestrian-level wind speed on the leeward outdoor space if building separation is incorporated with building setback.
(4) Wind permeability in the podium layer is very useful in leading airflow into deep street canyons. The building void between towers and podiums in Case 6 significantly accelerates turbulent flows in the podium layer, and the stepped podiums lead airflow into the pedestrian level. Airflow across the building void (10 m) is numerically presented by the red lines in Fig. 5.8. The mean wind speed on the leeward outdoor space can be improved to recreate the condition in Case 1903.
(5) Air passages should be arranged as close to the ground level as possible. Poor wind performance in Case 7 indicates that wind permeability in towers does not improve the pedestrian-level wind environment. Furthermore, compared with the profiles of Case 6, wind passage in the podium layer should incorporate the stepped podium to benefit the pedestrian-level wind environment, or the openings on the facade should be opened from the ground.
(6) Building setback, separation, and building permeability are useful in improving the pedestrian-level wind environment. However, the efficiency levels of these strategies differ. The consideration of urban area as a whole is important as natural ventilation performance in urban area results from the integral effects of buildings. Thus, air paths in these areas can be efficiently established and organized by applying different strategies to improve building porosity. Combining strategies (i.e., urban planning + building design) is recommended for the doubled benefits and efficiency over any single strategy. Planners and architects should choose appropriate strategies based on the actual design requirements and the insights from this Chapter.

(7) The current study gives scientific insights into the urban ventilation section of the Hong Kong Planning Standards and Guidelines (HKPSG) (HKPD 2011), as the Guidelines stress the importance to design urban breezeway and air path with nonbuilding areas and building setbacks from streets. Proper street alignment and sufficient open spaces that can be interlinked are equally important, as well as integration of the urban planning efforts into building-level designs. Building gaps, separations, and porosity close to the pedestrian levels are extremely useful in improving air space for urban air ventilation circulation.

(8) Increasing urban density has gained attention in recent worldwide discussions. Traditional wisdom attributes the decline of urban air ventilation to increasing urban density because of high urban frontal area density (FAD). While this understanding is generally correct, balancing the need to reduce land resources demand with designing more compact cities is also useful. The current study provides important insights on fine-tuning and designing urban morphologies and building forms that optimize urban air ventilation. Such optimization process can further incorporate the bio-meteorological needs of air ventilation in different climatic zones (Cheng et al. 2011).

(9) Evidence-based decision-making is important, especially for market or policy transformation (Ng 2010; Mills et al. 2010). This understanding is only possible with scientific and parametric studies that examine the sensitivity and performance of various design and planning options. The parameters should be defined carefully and practically to produce realistic results.

References

Ashie Y, Hirano K, Kono T (2009) Effects of sea breeze on thermal environment as a measure against Tokyo's urban heat island. Paper presented at the seventh international conference on urban climate, Yokohama, Japan

Betanzo M (2007) Pros and cons of high density urban environments. Build 39–40

Blocken B, Carmeliet J, Stathopoulos T (2007) CFD evaluation of wind speed conditions in passages between parallel buildings—effect of wall-function roughness modifications for the atmospheric boundary layer flow. Wind Eng Indus Aerodyn 95:941–962

Cheng V, Ng E (2006) Thermal Comfort in urban open spaces for Hong Kong. Architectural Sci Rev 49(2):179–182

Cheng V, Ng E, Chan C, Givoni B (2011) Outdoor thermal comfort study in a subtropical climate: a longitudinal study based in Hong Kong. Int J Biometeorol 13(4):586–594

Ferziger JH, Peric M (2002) Computational method for fluid dynamics, 3rd edn. Springer, Berlin

Fluent I (2006) FLUENT 6.3 User's Guide, pp 12–58

Hong Kong Planning Department (HKPD) (2005) Feasibility study for establishment of air ventilation assessment system, Final report. The government of the Hong Kong Special Administrative Region

Hong Kong Planning Department (HKPD) (2011) Hong Kong planning standards and guidelines. Hong Kong Special Administrative Region

Hoppe P (1999) The physiological equivalent temperature—a universal index for the biometeorological assessment of the thermal environment. Int J Biometeorol 43:71–75
Kleissl J, Parlange MB (2004) Field experimental study of dynamic smagorinsky models in the atmospheric surface layer. J Atmos Sci 61:2296–2307
Kondo H, Asahi K, Tomizuka T, Suzuki M (2006) Numerical analysis of diffusion around a suspended expressway by a multi-scale CFD model. Atomospheric Environ 42(38):8770–8784
Kuznik F, Brau J, Rusaouen G (2007) A RSM model for the prediction of heat and mass transfer in a ventilated room. Build Simul 919–926
Lawson T (2001) Building aerodynamics. Imperical College Press, London
Letzel MO, Krane M, Raasch S (2008) High resolution urban large-eddy simulation studies from street canyon to neighbourhood scale. Atmos Environ 42(38):8770–8784
Meneveau C, Katz J (2000) Scale-Invariance and turbulence models for large-eddy simulation. Annu Rev Fluid Mech 32:1–32
Menter FR, Kuntz M, Langtry R (2003) Ten years of industrial experience with the SST turbulence model. Turbul Heat Mass Transfer 4:625–632
Mills G, Cleugh H, Emmanuel R, Endlicher W, Erell E, McGranahan G, Ng E, Nickson A, Rosenthal J, Steemers K (2010) Climate information for improved planning and management of mega cities (needs perspective). Procedia Environ Sci 1:228–246
Mochida A, Murakami S, Ojima T, Kim S, Ooka R, Sugiyama H (1997) CFD analysis of mesoscale climate in the Greater Tokyo area. J Wind Eng Ind Aerodyn 67–68:459–477
Mochida A, Tominaga Y, Murakam S, Yoshie R, Ishihara T, Ooka R (2002) Comparison of various κ-ε models and DSM applied to flow around a high-rise building—report on AIJ cooperative project for CFD prediction of wind environment. Wind Struct 5(2–4):227–244
Moss P (2008) Hong Kong an affair to remember. FromAsia Books Limited, Hong Kong
Murakami S (2006) Environmental design of outdoor climate based on CFD. Fluid Dyn Res 38(2–3):108–126
Murakami S, Deguchi K (1981) New criteria for wind effects on pedestrians. Wind Eng Indus Aerodyn 7:289–309
Ng E (2009a) Designing high-density cities. Earthscan, London Sterling
Ng E (2009b) Policies and technical guidelines for urban planning of high density cities—air ventilation assessment (AVA) of Hong Kong. Build Environ 44 (1478–1488)
Ng E (2010) Towards a planning and practical understanding for the need of meteorological and climatic information for the design of high density cities—a case based study of Hong Kong. Int J Climatol
Ng E, Cheng V, Chan C (2008) Urban climatic map and standards for wind environment—feasibility study. Technical input report no. 1: Methodologies and finds of user's wind comfort level survey. Hong Kong Planning Department, Hong Kong
Ng E, Yuan C, Chen L, Ren C, Fung JCH (2011) Improving the wind environment in high-density cities by understanding urban morphology and surface roughness: a study in Hong Kong. Landscape Urban plan 101(1):59–74
Oke TR (2006) Initial guidance to obtain representative meteorological observations at urban sites. World Meteorological organization, Switzerland
Stathopoulos T, Storms R (1986) Wind environmental conditions in passages between buildings. Wind Eng Indus Aerodyn 95:941–962
To AP, Lam KM (1995) Evaluation of pedestrian-level wind environment around a row of tall buildings using a quartile-level wind speed descriptor. Wind Eng Indus Aerodyn 54–55:527–541
Tominaga Y, Mochida A, Yoshie HK, Nozu T, Yoshikawa M, Shirasawa T (2008) AIJ guidelines for practical applications of CFD to pedestrian wind environment around buildings. J Wind Eng Ind Aerodyn 96:1749–1761

United Nations Population Division (2006) World urbanization prospects: the 2005 revision. United Nations, New York
Waller J (2008) Hong Kong the growth of the city. Compendium Publishing, London, United Kingdom
Wikipedia (2011) Mong Kok. http://en.wikipedia.org/wiki/Mong_Kok
Wolf M (2009) Hong Kong outside. Asia One Books and Peperoni Books, Hong Kong
Wong FJ (2004) Computational fluid dynamics analysis. Tsinghua University Press, Beijing
World Wildlife Fund (WWF) (2010) Hong Kong ecological footprint report 2010—paths to a sustainable future
Yim SHL, Fung JCH, Lau AKH (2009a) Mesoscale simulation of year-to-year variation of wind power potential over southern China. Energies 2:340–361
Yim SHL, Fung JCH, Lau AKH, Kot SC (2009b) Air ventilation impacts of the "wall effect" resulting from the alignment of high-rise buildings. Atomospheric Environ 43(32):4982–4994